




Article

Tetraphenylethylene-Substituted Bis(thienyl)imidazole (DTITPE), An Efficient Molecular Sensor for the Detection and Quantification of Fluoride Ions

Ranjith Kumar Jakku^{1,2,3}, Nedaossadat Mirzadeh^{2,3}, Steven H. Privér³, Govind Reddy^{3,4} , Anil Kumar Vardhaman⁴, Giribabu Lingamallu^{2,4,5} , Rajiv Trivedi^{1,2,5} and Suresh Kumar Bhargava^{2,3,*} 

- ¹ Catalysis and Fine Chemicals Division, CSIR-Indian Institute of Chemical Technology, Uppal Road, Tarnaka, Hyderabad 500007, India; ranjithkumar4chem@gmail.com (R.K.J.); trivedi@csiriict.in (R.T.)
- ² IICT-RMIT Centre, CSIR-Indian Institute of Chemical Technology, Uppal Road, Tarnaka, Hyderabad 500007, India; nedaossadatmirzadeh@gmail.com (N.M.); giribabu@iict.res.in (G.L.)
- ³ Centre for Advanced Materials and Industrial Chemistry (CAMIC), School of Science, RMIT University, GPO Box 2476, Melbourne 3001, Australia; steven.priver@rmit.edu.au (S.H.P.); r.govindreddy@gmail.com (G.R.)
- ⁴ Polymer and Functional Materials Division, CSIR-Indian Institute of Chemical Technology, Uppal Road, Tarnaka, Hyderabad 500007, India; anil1hnk@gmail.com
- ⁵ Academy of Scientific and Innovative Research, AcSIR Headquarters, CSIR-HRDC Campus Sector 19, Kamala Nehru Nagar, Ghaziabad 201002, India
- * Correspondence: suresh.bhargava@rmit.edu.au; Tel.: +61-3-9925-2330



Citation: Jakku, R.K.; Mirzadeh, N.; Privér, S.H.; Reddy, G.; Vardhaman, A.K.; Lingamallu, G.; Trivedi, R.; Bhargava, S.K. Tetraphenylethylene-Substituted Bis(thienyl)imidazole (DTITPE), An Efficient Molecular Sensor for the Detection and Quantification of Fluoride Ions. *Chemosensors* **2021**, *9*, 285. <https://doi.org/10.3390/chemosensors9100285>

Academic Editors: Valerio Vignoli and Enza Panzardi

Received: 23 July 2021

Accepted: 28 September 2021

Published: 6 October 2021

Publisher's Note: MDPI stays neutral with regard to jurisdictional claims in published maps and institutional affiliations.



Copyright: © 2021 by the authors. Licensee MDPI, Basel, Switzerland. This article is an open access article distributed under the terms and conditions of the Creative Commons Attribution (CC BY) license (<https://creativecommons.org/licenses/by/4.0/>).

Abstract: Fluoride ion plays a pivotal role in a range of biological and chemical applications however excessive exposure can cause severe kidney and gastric problems. A simple and selective molecular sensor, 4,5-di(thien-2-yl)-2-(4-(1,2,2-triphenylvinyl)-phenyl)-1H-imidazole, DTITPE, has been synthesized for the detection of fluoride ions, with detection limits of 1.37×10^{-7} M and 2.67×10^{-13} M, determined by UV-vis. and fluorescence spectroscopy, respectively. The variation in the optical properties of the molecular sensor in the presence of fluoride ions was explained by an intermolecular charge transfer (ICT) process between the bis(thienyl) and tetraphenylethylene (TPE) moieties upon the formation of a N-H—F[−] hydrogen bond of the imidazole proton. The sensing mechanism exhibited by DTITPE for fluoride ions was confirmed by ¹H NMR spectroscopic studies and density functional theory (DFT) calculations. Test strips coated with the molecular sensor can detect fluoride ions in THF, undergoing a color change from white to yellow, which can be observed with the naked eye, showcasing their potential real-world application.

Keywords: bis(thienyl) imidazole; tetraphenylethylene; molecular sensor; fluoride anion; fluorescence

1. Introduction

The detection and recognition of anionic analytes has developed into an extremely active research field in recent years [1–14]. Anions play a crucial role in a range of biological and chemical processes, and their detection, even at extremely low concentrations, has been the motivation for continuous improvement in sensor development over the last few decades [15,16]. According to the previous literature, the probable toxic dose (PTD) of fluoride was defined at 5 mg/kg of body mass. The PTD is the minimal dose that could trigger serious and life-threatening signs and symptoms which require immediate treatment and hospitalization [17]. The fluoride anion, having the smallest ionic radii, hard Lewis basic nature and high charge density, has emerged as an appealing subject for sensor design due to its association with a wide range of organic, medicinal, and technological procedures.

Moreover, fluoride ions play a significant role in dental health [18] and has been utilized for the treatment of osteoporosis [19–21] and for military uses, including the refinement of uranium for nuclear weapons [22]. It is readily absorbed by the human body

but is only discharged slowly, therefore continuous exposure to fluoride can cause serious kidney and gastric issues. Despite recent progress in the development of molecular sensors, highly anion-selective sensors remain a challenge. Several fluoride detection techniques, such as ^{19}F NMR spectroscopic analysis [23], titrimetric, voltametric, potentiometric, and electrochemical methods, as well as ion-exchange chromatography, frequently show high detection limits [24–30]. However, these methods have significant drawbacks associated with the requirements of delicate instrumentation and tedious manipulations [31]. Additionally, ^{19}F NMR spectroscopy is only able to detect fluoride up to micromolar levels. Moreover, neither the spectroscopic nor electrochemical methods can be miniaturized for use in the investigation of *in vivo* biological processes.

In 2001, Tang and co-workers reported the aggregation-induced emission (AIE) of 1-methyl-1,2,3,4,5-pentaphenylsilole which provided new guidance in the design of fluorescent probes [32]. Many fluorescent sensors based on AIE have been developed to detect acidity/basicity, explosives, carbohydrates, proteins, and anions [33–36]. AIE-active fluorescent molecular sensors can be used in aqueous media and offer good practical use in biological systems. Tetraphenylethylene (TPE) is one of the most prominent and extensively modified scaffolds for use in AIE applications [37–44].

Simple organic molecules containing imidazole rings possess binding sites which can behave as selective and highly sensitive molecular sensor systems (Figure 1). The imidazole proton can function as an excellent hydrogen bond donor for anion sensing, the acidity of which can be regulated by changing the electronic properties of the substituents on the imidazole ring [45]. Due to their good accessibility, imidazole compounds have been widely used as a supramolecular chemistry [46], and photoelectric material [47]. The emissive properties of imidazole derivatives enhance their utility in fluorescence studies [48] and some examples of imidazole-based molecular sensor for the detection of fluoride ions are shown in Figure 1. The tri-benzimidazolyl star-shaped molecules 1a are deprotonated by fluoride ions, resulting in a color change from blue to light cyan [49]. In the presence of fluoride (or copper ions), solutions of the β -carboline-imidazopyridine hybrid 1b undergo significant changes in their absorption and emission spectra, corresponding to color change from colorless to yellow [50]. In polar organic solvents, the compound (9H-pyreno[4,5-d]imidazole-10-yl)-4-benzaldehyde 1c can efficiently detect fluoride ions at sub-millimolar levels; hydrogen bond formation and subsequent deprotonation takes place, resulting in a significant colorimetric response. Fluorescence studies indicates the sensing ability of the compound is via intramolecular charge transfer (ICT) processes [51]. Similarly, 2-(2-thienyl)-1-H-naphtho[2,3-d]imidazole-4,9-dione 1d from hydrogen bonds with fluoride (or cyanide) ions and undergo a bathochromic shift characteristic ICT transition bond [52].

According to Ye's investigation, refs. [45,53,54] the mechanism behind the anion sensing ability of imidazole-based sensors is via the formation of $\text{N-H}\cdots\text{X}^-$ hydrogen bonds or by deprotonation (mono-proton transfer), resulting in changes to their optical properties. Fluoride ions have a strong affinity towards the N-H group, promoting hydrogen bonding with the imidazole molecular sensor. Supported by density functional theory (DFT) and time-dependent density functional theory (TD-DFT) studies, imidazole rings containing fluorophores have been shown to act selectively as fluoride sensors via hydrogen bond formation and, in some cases, subsequent deprotonation [45,53,54]. In an effort to combine the desirable properties of tetraphenylethylene and imidazole moieties for the development of highly selective sensors, the present work describes the synthesis, characterization and optoelectronic properties of a TPE-linked bis(thienyl) imidazole derivative and its application as a fluoride sensor.

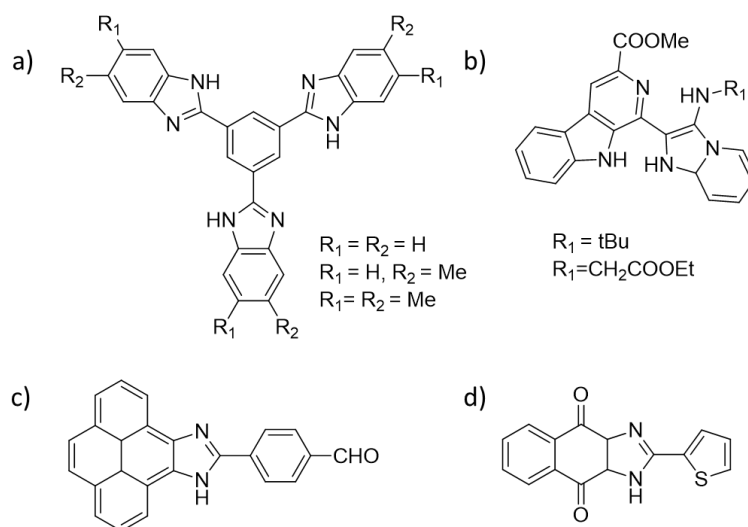


Figure 1. Examples of (a) tri-benzimidazolyl-, (b) β-carboline-imidazopyridine-, (c) pyrenoimidazolyl-, and (d) naphthoimidazole dione-based molecular sensors used for fluoride detection.

2. Materials and Methods

All chemicals were obtained from Sigma Aldrich (St. Louis, MO, USA) and used as received. Tetrahydrofuran was used for the sensing experiments, which was freshly dried and distilled prior to use. ¹H and ¹³C NMR spectra were recorded on Bruker Avance 400, Varian Inova 500 or Bruker Avance 300 MHz spectrometer (Karlsruhe, Germany) at room temperature. Chemical shifts (δ) are reported in ppm and referenced to TMS (¹H) or residual solvent signals (¹³C) and coupling constants (J) are reported in Hz. Mass spectra were obtained using a Bruker Autoflex Speed (MALDI-TOF, Karlsruhe, Germany) or Water Quattro Micro (ESI) spectrometer (Karlsruhe, Germany). UV-vis. spectra were recorded on an Agilent Cary 60 spectrometer in the range of 200–600 nm as THF solutions. FT-IR spectra were recorded on a Perkin Elmer Spectrum (Akron, OH, USA) 100 spectrometer as KBr discs.

2.1. Computational Methods

Computational calculations were performed using the Gaussian 09 software suite. The initial geometries of the DTITPE probe were constructed using Gauss View 05 and optimized using the DFT/Becke, 3-parameter, lee–yang–parr(B3LYP)/6-31+G(d,p) level in the gas phase. The optimized stable DTITPE structure was used to construct the new structures of DTITPE.F[−], and DTITPE[−] which were then optimized using the same methods. The frequency calculations indicated the presence of a local minimum state. Further, the stable geometries were used for the calculation of excitation parameters using the TDDFT/B3LYP(6-31+G(d,p))/conductor-like polarizable continuum model (CPCM) method in THF. Major portions of the absorption spectra for the interpretation of orbital transitions were acquired using the GaussSum 2.2.5 software package. The contribution percentages of the individual units present in the molecular probes to the respective molecular orbitals were calculated [55].

2.2. Synthesis of 4-(1,2,2-Triphenylvinyl)benzaldehyde

To a mixture of 4-(4,4,5,5-tetramethyl-1,3,2-dioxaborolan-2-yl)benzaldehyde (0.9 g, 6.0 mmol), 2-bromo-1,1,2-triphenylethylene (1.6 g, 5.0 mmol) and tetrabutylammonium bromide (1.61 g, 5.0 mmol) in a 50 mL round-bottom flask was added toluene (25 mL) and aqueous Na₂CO₃ solution (2.0 M, 6 mL). [Pd(PPh₃)₄] (104 mg, 0.1 mmol) was then added and the mixture was vigorously stirred under nitrogen at 90 °C for 16 h. After cooling to room temperature, the reaction mixture was extracted with dichloromethane and the solvents removed by evaporation. The crude solid residue was purified by column

chromatography (silica gel), eluting with hexane/dichloromethane (1:1) to give, after work up, 1.35 g of product as a yellow solid. Yield: 75%. ^1H NMR (500 MHz, CDCl_3): δ 9.93 (s, 1H, CH), 7.64 (d, $J = 8.3$ Hz, 2H, Ar H), 7.22 (d, $J = 8.2$ Hz, 2H, Ar H), 7.17–7.11 (m, 10H, Ar H), 7.07–7.02 (m, 5H, Ar H). ^{13}C NMR (75 MHz, CDCl_3): δ 191.86, 150.57, 143.07, 143.03, 142.92, 139.80, 134.33, 131.96, 131.30, 131.26, 130.90, 129.17, 127.95, 127.77, 127.08, 126.90. ESI-MS (m/z): 361 $[\text{M}+\text{H}]^+$.

2.3. Synthesis of 4,5-Di(thien-2-yl)-2-(4-(1,2,2-triphenylvinyl)phenyl)-1H-Imidazole (DTITPE)

In a 100 mL round-bottom flask fitted with an efficient reflux condenser were placed 4-(1,2,2-triphenylvinyl)benzaldehyde (0.36 g, 1 mmol), 1,2-di(thienyl-2-yl)ethane-1,2-dione (0.22 g, 1 mmol), and ammonium acetate (1.15 g, 15 mmol). Glacial acetic acid (15 mL) was added and the solution was stirred at reflux for 12 h. The reaction mixture was cooled to room temperature and poured into ice-cold water. The precipitated solid was isolated by filtration, washed sequentially with water and diethyl ether then dried under reduced pressure. The crude product was purified by column chromatography, eluting with 1:1 ethyl acetate/dichloromethane to give 0.8 g of product as a colorless solid. Yield: 85%. ^1H NMR (CDCl_3 , 400 MHz): δ 9.30 (s, 1H, imidazole NH), 7.61–7.59 (d, $J = 8.2$ Hz, 2H), 7.38 (s, 1H, CH), 7.10 (td, $J = 6.1, 3.3$ Hz, 15H), 7.06–7.02 (m, 7H). ^{13}C NMR (CDCl_3 , 75 MHz): δ 146.01, 143.52, 143.34, 140.21, 132.00, 131.43, 131.38, 131.34, 127.89, 127.80, 127.72, 126.74, 126.68, 124.79. IR (KBr, cm^{-1}): 3380, 2976, 1567, 1444, 1269, 1076, 904, 698; MALDI-TOF (m/z): 563.6 $[\text{M}+\text{H}]^+$

2.4. UV-Vis. and Fluorescence Studies

DTITPE (1.68 mg, 1 mmol) was dissolved in THF (3 mL) and a 9 μL aliquot of this solution was diluted to 3 mL with THF to give a final stock solution concentration of 1 μM . A stock solution of tetra-*n*-butylammonium fluoride (TBAF) (0.1 mM) was prepared in anhydrous THF. Aliquots of the THF stock solutions of DTITPE and TBAF were combined and thoroughly mixed at room temperature and their fluorescence emission spectra (400–650 nm) recorded upon excitation at 360 nm, and also UV-vis. spectra was collected.

2.5. Determination of Association Constants

The association constant of the DTITPE. F^- adduct was determined using fluorescence and UV-vis. absorption spectroscopy and the Benesi–Hildebrand Equations (1) and (2)

$$1/(A - A_0) = 1/\{K(A_{\text{max}} - A_0) C\} + 1/(A_{\text{max}} - A_0) \quad (1)$$

$$1/(I - I_0) = 1/\{K(I_{\text{max}} - I_0) C\} + 1/(I_{\text{max}} - I_0) \quad (2)$$

where A and A_0 are the absorbances at 405 nm in the presence and absence of fluoride ions, respectively, and A_{max} is the maximum absorbance when various concentrations of F^- were titrated to the sensor DTITPE solution. Similarly, I and I_0 are the emissions at 635 nm in the presence and absence of fluoride ions, respectively, and I_{max} is maximum emission when various concentrations of F^- were titrated to the sensor DTITPE solution. K is the association constant, determined from the plots of the reciprocal concentration and change in absorbance or emission graphs.

2.6. Determination of Detection Limits and Quantification Limits for DTITPE

The detection limits and quantification limits of DTITPE for fluoride ion were determined using UV-vis. and fluorescence titration data. Using Equations (3) and (4), where σ is the standard deviations (obtained from the average of 10 titrations of the sensor and the fluoride ion solution) and k is the slope from the plot of concentration of fluoride ion versus absorbance of DTITPE.

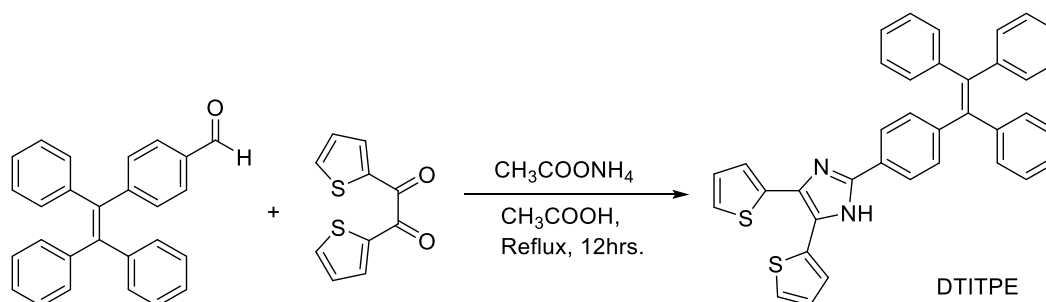
$$\text{Detection limit} = 3\sigma/k \quad (3)$$

$$\text{Quantification limit} = 10\sigma/k \quad (4)$$

3. Results

3.1. Synthesis and Characterization of DTITPE

The molecular sensor 4,5-di(thien-2-yl)-2-(4-(1,2,2-triphenylvinyl)-phenyl)-1H-imidazole (DTITPE) was synthesized via a condensation reaction between 4-(1,2,2-triphenylvinyl) benzaldehyde and 2,2'-thienil in the presence of ammonium acetate (Scheme 1) and isolated as a white solid in 85% yield.



Scheme 1. Synthesis of the molecular sensor DTITPE.

The ^1H NMR spectrum of DTITPE showed a broad singlet resonance at δ 9.30 due to the imidazole proton, and a doublet ($J = 8.2$ Hz) at δ 7.61, assignable to two protons of the substituted aryl ring of the tetraphenylethylene moiety. The resonances due to the remaining aromatic and thienyl protons appear as multiplets around δ 7.0–7.5. The MALDI-TOF mass spectrum of DTITPE showed the expected $[\text{M}+\text{H}]^+$ ion peak at m/z 563.6.

The molecular structure of DTITPE was also confirmed by single-crystal X-ray diffraction (Figure 2). Light-yellow colored square-shaped crystals of DTITPE, obtained from THF/hexane by slow evaporation, crystallized in the orthorhombic $Pna2_1$ space group (Table S4). The structure confirmed the presence of TPE with a di(thienyl) substituted imidazole group bound to one of the phenyl rings; the imidazole and attached phenyl ring are almost co-planar. In the structure of DTITPE, the thienyl group containing S1 was disordered by a 180° rotation about the C28–C30 bond. The bond lengths and angles in DTITPE are within normal ranges.

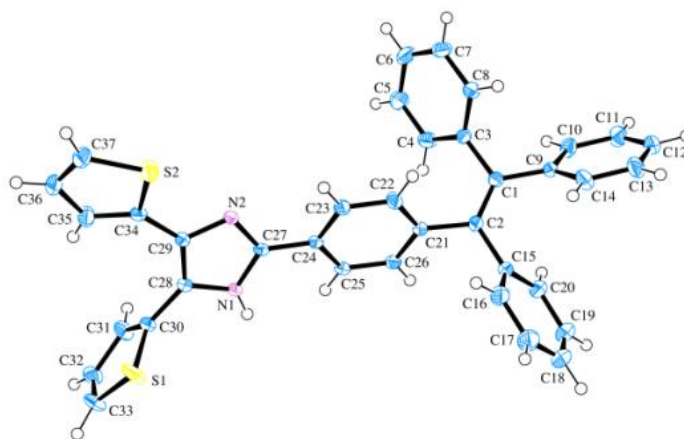


Figure 2. Molecular structure of DTITPE. Ellipsoids show 50% probability levels. The thienyl group containing S1 was disordered (0.749:0.251) by a 180° rotation about the C28–C30 bond and only the major position is shown.

Upon the addition of TBAF to a solution of DTITPE in THF, changes in the NMR spectrum were observed. The ^1H NMR spectrum showed the disappearance of the imidazole proton resonance as well as a downfield shift of the two *o*-phenyl proton resonances, from δ

7.61 to δ 8.10 ppm, due to a de-shielding effect, consistent with the formation of a hydrogen bond between the imidazole proton and fluoride ion (DTITPE.F⁻).

3.2. Optical Studies of the Molecular Sensor DTITPE

DTITPE is a stable compound as a solid and in solution, providing an ideal platform for performing sensing studies. The H-bonded DTITPE.F⁻ species formation was further supported by absorption and emission spectroscopic titrations. The UV-vis. and fluorescence emission spectrum of a 3×10^{-6} M solution of DTITPE in THF was monitored during the incremental addition of fluoride ions (2.3×10^{-7} to 5.1×10^{-6} M) and (3.0×10^{-7} to 9.0×10^{-6} M) respectively. Under ambient light, the addition of fluoride ions to a THF solution containing DTITPE resulted in a color change from colorless to yellow. The UV-vis. and fluorescence emission spectra were collected until no further spectral changes took place at a final fluoride ion concentration of 5×10^{-6} M.

The UV-vis. absorption spectrum of DTITPE in THF showed a band centered at 350 nm. No significant spectral changes were observed after the addition of THF solutions containing acetate, hydrogen sulfate, dihydrogen phosphate, iodide, bromide, or chloride ions (Figure 3a). In contrast, however, upon the incremental addition of tetrabutylammonium fluoride (TBAF) to the DTITPE solution, a gradual decrease in the intensity of the absorption band at 350 nm and the appearance of a new absorption band at 405 nm was observed (Figure 3b). From the intercept of the Benesi–Hildebrand plot of the UV data, the DTITPE versus fluoride association constant was found to be $3.30 \times 10^5 \text{ M}^{-1}$ at slope $k = 3.03 \times 10^{-6}$. The slope for the plot between the absorbance intensities at various concentrations of fluoride anion added to the sensor solution was calculated as $k = 6.55 \times 10^4$. Using Equation (3) and the UV-vis. spectroscopic titration data, the detection limit of DTITPE was found to be 1.37×10^{-7} M. The limit of detection of DTITPE is one order of magnitude less than those of related imidazole-derived chemosensors, such as the phenazine (1.8×10^{-6} M) [56] and anthraimidazole-dione-based (0.5×10^{-6} M) [57] fluoride sensors (See Table S4). Furthermore, using Equation (4) and the results from the UV-vis. titration experiments, the quantification limit of the DTITPE from UV-vis. data was calculated to be 4.58×10^{-7} M.

The fluorescence emission spectrum of DTITPE in THF showed an intense emission band at 510 nm (Figure 3c) when excited at 345 nm. From the intercept of the Benesi–Hildebrand plot of the fluorescence data, the association constant for DTITPE towards fluoride ions was found to be $4.38 \times 10^5 \text{ M}^{-1}$ at slope $k = 2.28 \times 10^{-6}$. The emission spectra of the sensor solution were also recorded, and the standard deviation was found to be $\sigma = 0.003$. Plotting the fluorescence intensities against various concentrations of F⁻, the slope was found to be $k = 3.00 \times 10^{10}$. The detection limit of DTITPE was calculated to be 3.00×10^{-13} M using the results of the fluorescence spectroscopic titration experiment. Furthermore, the quantification limit of DTITPE was calculated to be 1.00×10^{-12} M.

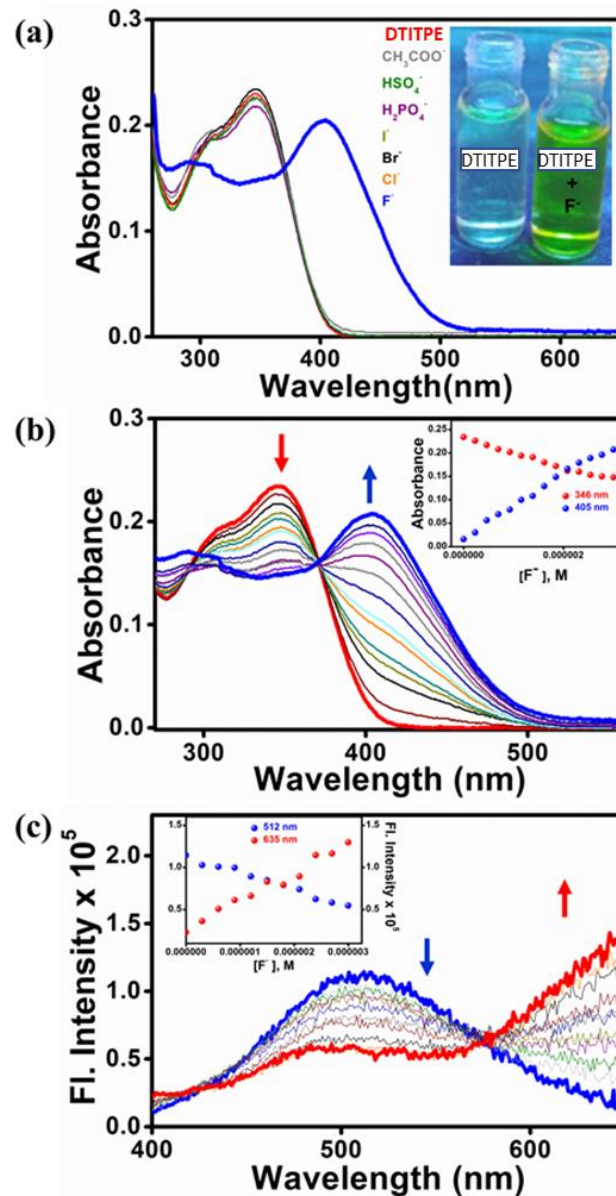


Figure 3. (a) UV-vis. spectra of a THF solution of DTITPE (3×10^{-6} M) in the absence and presence of various anions. (b) UV-vis. titration spectra of DTITPE in THF (3×10^{-6} M) upon incremental addition of TBAF solutions (2.31×10^{-7} to 5×10^{-6} M). (c) Fluorescence emission titration spectra of DTITPE (3×10^{-6} M) upon incremental addition of TBAF (3×10^{-7} to 9×10^{-6} M).

3.2.1. Aggregation Induced Emission (AIE)

To determine if DTITPE exhibited aggregation induced emissive (AIE) properties, solutions of the 1×10^{-5} M of DTITPE in THF containing 0 to 90% of water (by volume) were prepared. Under UV irradiation the solutions were weakly emissive, the intensity of which increased with increasing water fraction (f_w) (Figure 4a); a similar trend was also observed in the fluorescence spectra of the solutions (Figure 4b) upon excitation at 360 nm. Solutions containing up to 70% water only showed a low intensity band centered around 540 nm. At $f_w = 80\%$, the fluorescence intensity increased significantly, which increased further at $f_w = 90\%$ due to restricted rotation of the phenyl rings of the tetraphenyl ethylene moiety.

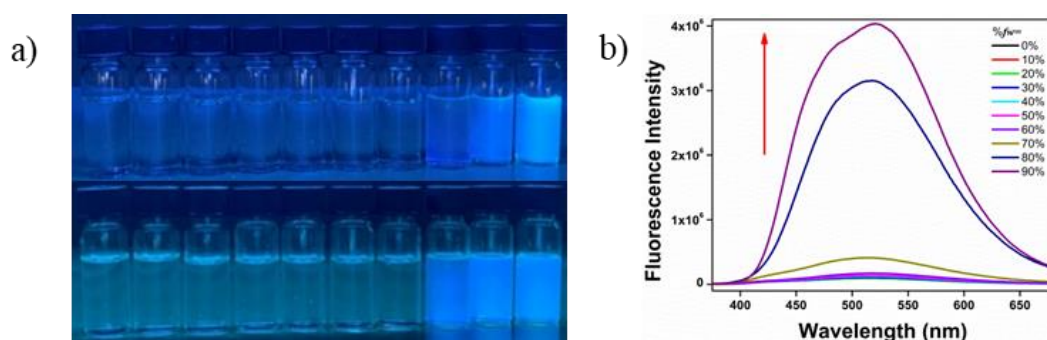


Figure 4. (a) Solutions of DTITPE (1×10^{-5} M) in THF containing, from left to right, increasing amounts of water (f_w , 0–90 vol%) under UV irradiation (top: 185 nm; bottom 365 nm). (b) Fluorescence emission spectra of DTITPE (1×10^{-5} M) in THF containing increasing amounts of water (f_w , vol%).

3.2.2. Mechanochromism

Mechano-responsive luminescent materials containing AIE moieties exhibit tunable emissions by the application of an external stimuli, ref. [58] such as mechanical stress. Such materials are of significant interest due to their wide-ranging applications in mechano-sensors, optical storage, security papers, miniature photonic devices and logic gates [59–62]. In the solid state, DTITPE exhibits mechanochromic behavior. Under UV irradiation (365 nm) at ambient temperature, DTITPE emits blue light, with an emission maximum at 448 nm. Upon grinding, the emission is red-shifted to 479 nm and green light is emitted (Figure 5). This process is reversible, and in the presence of dichloromethane vapor the original blue light is restored.

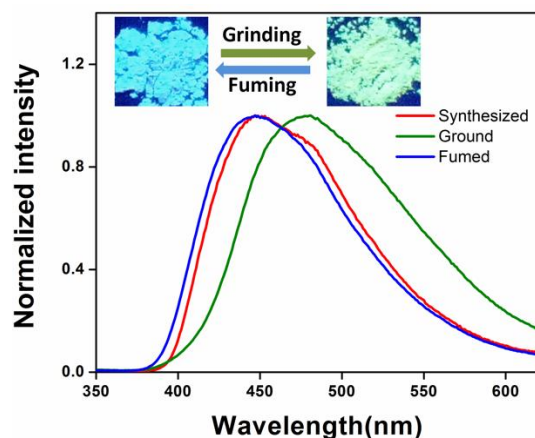


Figure 5. Fluorescence emission spectra of DTITPE as synthesized (red line), after grinding (green line) and after exposure to CH_2Cl_2 vapor (blue line). Inset: photographs of the ground and CH_2Cl_2 -fumed solids under UV irradiation (365 nm).

3.3. Computational Studies

In order to understand the electronic structure and the distribution of electron density in DTITPE, both before and after interaction with fluoride ions, DFT calculations were performed using Gaussian 09 software at the B3LYP/6-31+G(d,p) level. Absorption spectra were also simulated using the CPCM method with THF as solvent (Figure S23). The optimized geometries of the parent DTITPE molecule, DTITPE containing an imidazole hydrogen–fluoride interaction (DTITPE.F[−]), and the deprotonated sensor (DTITPE)[−] in the gaseous phase are shown in Figures S17, S19 and S21, respectively, and the electrostatic potential (ESP) maps and the corresponding frontier molecular orbitals are shown in

Figures S18, S20 and S22, respectively. The calculated bond lengths and dihedral angles of DTITPE, DTITPE.F⁻ and DTITPE⁻ are shown Table S1.

In DTITPE, the imidazole N-H bond length was calculated to be 1.009 Å, which elongated to 1.474 Å in the presence of F⁻ ion as a result of hydrogen bond formation to give the complex DTITPE.F⁻ (Figure 6). In the adduct DTITPE.F⁻ (Scheme 2), the H—F bond length was calculated to be 1.025 Å, significantly shorter than characteristic H—F bond lengths, which typically range between 1.73 to 1.77 Å [63,64]. From geometrical aspects, it can be seen that the DTITPE, DTITPE.F⁻, and DTITPE⁻ molecules are non-planar in nature with the tetraphenyl groups as well as the two thienyl groups existing in two different planes (Table S1) [65]. In each compound, the dihedral angle between two *cis*-oriented phenyl rings in the TPE moieties range from ~11.9° to 14.09°, whereas the angle between two *trans*-oriented groups ranges from ~-165.8° to -167.8° (Figures S17, S19 and S21).

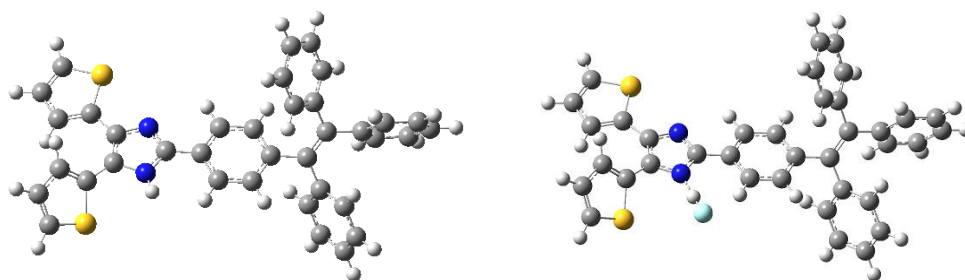
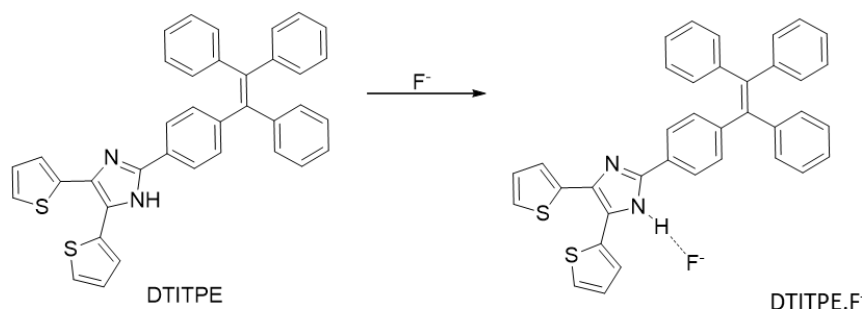


Figure 6. Optimized geometric structures of DTITPE (left) and DTITPE.F⁻ (right), showing the elongation of the imidazole N-H bond length upon interaction with fluoride.



Scheme 2. Plausible reactivity of DTITPE towards fluoride ions.

The frontier molecular orbital (FMO) of DTITPE (Figure S18) indicates that the electron density distribution in the HOMO is mostly located on the bis(thienyl) imidazole and di-substituted benzene ring, whereas in the LUMO, it is mainly located over the entire molecule except for one thienyl group. In the case of the hydrogen bonded species DTITPE.F⁻ (Figure S20), the electron density distribution in the HOMO is mostly located on the bis(thienyl) imidazole ring while in the LUMO, it is mostly found on the tetraphenylethylene moiety. In DTITPE⁻ (Figure S22), the electron density distribution pattern in both the HOMO and LUMO are similar to that in the hydrogen bonded DTITPE.F⁻ analogue (Figure S20). These results suggest that the hydrogen bonded DTITPE.F⁻ and the deprotonated DTITPE⁻ species undergo a charge transfer from the HOMO to the LUMO [65]. More precisely, they both exhibit intramolecular charge transfer (ICT) from the bis(thienyl) imidazole ring to the tetraphenyl ethylene unit. The calculated band gaps (ΔE) between the HOMO and LUMO of the DTITPE, hydrogen bonded DTITPE.F⁻, and deprotonated DTITPE⁻ were found to be 3.42, 2.38, and 1.25 eV, respectively (Table S2). This red-shift was observed in the theoretical UV-vis. spectrum for DTITPE upon formation of a hydrogen bond with F⁻, as shown in Figure S23 and Table S3, which is in good agreement with experimental results (Figure 3). The electron distribution in the molecule is altered as

a result of the hydrogen bond, which improves the push-pull effect of an intramolecular charge transfer (ICT) process [54]. Additionally, the abstraction of the imidazole N-H proton decreased the bandgap, which would suggest a red-shift of the peak maxima in its DFT absorption spectrum [65]. Moreover, DTITPE optimized geometry was further used for the calculation of excitation parameters using the TD-DFT. The computation revealed that the observed absorption band in DTITPE is caused by the transition from HOMO to LUMO orbitals (So to S1) (Figure 3 and Figure S23, Table S3). The most stable geometry of the DTITPE.F⁻ and DTITPE⁻ were used to calculate the excitation parameters and their results suggested that HOMO-1 to LUMO, HOMO to LUMO+1, and HOMO-4 to LUMO orbitals are responsible for the observed singlet electronic observed in DTITPE.F⁻ and DTITPE⁻ (Figure 7, Figures S18, S20 and S22, and Table S3). The TD-DFT calculations indicated that there is decrease in the ground state to the excited state gap, which causes a bathochromic shift.

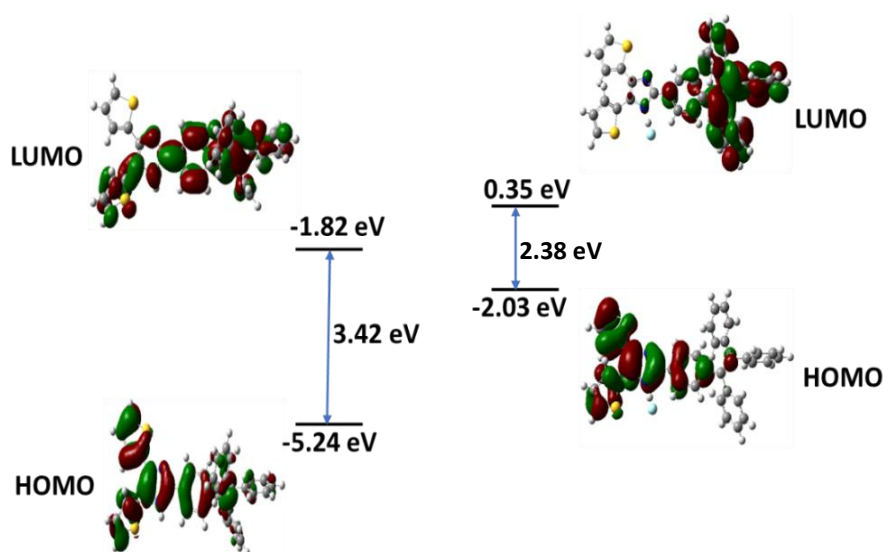


Figure 7. Energy levels diagram of DTITPE and DTITPE.F⁻ calculated by DFT.

From the electrostatic potential maps (ESP) (Figures S17b, S19b and S21b), the most electronegative portion of DTITPE is located near the imidazole ring nitrogen, both before and after interaction with fluoride, and the dipole moment increases from ~3.1 D for DTITPE to ~12 D for DTITPE.F⁻ (Table S2). This could be useful to assist molecular packing and would also be expected to augment intermolecular charge transport (ICT) processes [66].

3.4. Detection of F⁻ Anions Using a Silica Gel Dip-Strip Method

The promising result that a THF solution of DTITPE underwent a color change in the presence of fluoride ions (Figure 8a) prompted us to investigate its potential application to in-field sensing devices. Silica gel sheets were treated with 1×10^{-5} M solutions of DTITPE by a dip-coating method and the solvent was allowed to evaporate. Immersion of the test strips into THF solutions containing OAc⁻, H₂PO₄⁻, HSO₄⁻, Cl⁻, Br⁻, or I⁻ ions showed no obvious changes, however upon immersion into a solution containing F⁻ ions, the test strip underwent a color change from white to yellow within seconds, which could be observed with the naked eye (Figure 8b). Under UV irradiation (254 nm), a color change from blue to light yellow was observed for test strips exposed to fluoride ions (Figure 8c). These results are very promising for the use of DTITPE in selective sensing devices for the real time detection of fluoride ions in THF solution.

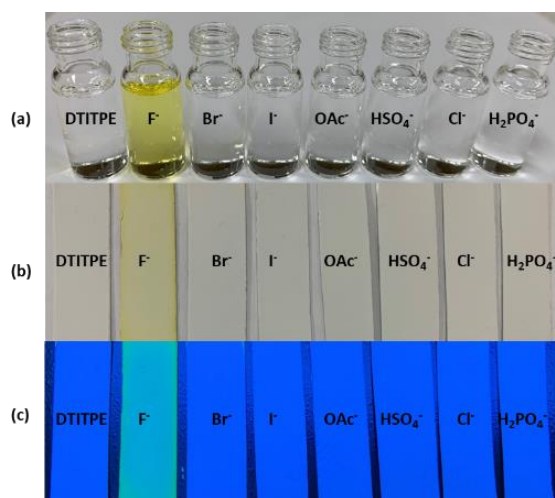


Figure 8. Color change of 1×10^{-5} M of DTITPE in the presence of various anions (a) in THF solution, and on silica gel strips under (b) ambient light and (c) UV irradiation (254 nm).

4. Conclusions

In conclusion, the molecular sensor DTITPE was synthesized and fully characterized. In the presence of fluoride ions, a colorless solution of DTITPE immediately turned yellow and from a Job's plot experiment, a 1:1 stoichiometric ratio between DTITPE and F⁻ ion was determined. These results are consistent with the formation of a species containing a hydrogen bond between the imidazole proton of DTITPE and the fluoride ion, a conclusion which was supported by NMR spectroscopic results and DFT calculations. Using UV-vis. and fluorescence emission spectroscopy, fluoride detection limits of DTITPE were calculated to be 1.37×10^{-7} and 3.00×10^{-13} M, respectively. Furthermore, using the Benesi–Hildebrand equation, the association constants were found to be $K = 3.30 \times 10^5$ M⁻¹ and 4.38×10^5 M⁻¹, as determined from the UV-vis. and fluorescence emission data, respectively. Moreover, DTITPE was successfully applied to a silica gel dip strip which could be used to selectively detect fluoride ions in solution.

Supplementary Materials: The following are available online at <https://www.mdpi.com/article/10.3390/chemosensors9100285/s1>, Figure S1: ¹H NMR spectrum of 4-(1,2,2-triphenylvinyl) benzaldehyde (400 MHz, CDCl₃): δ 9.90 (s, 1H), 7.62 (d, 2H), 7.21 – 7.18 (m, 2H), 7.12 (dd, *J* = 3.7, 3.2 Hz, 9H), 7.01 (ddt, *J* = 4.7, 2.3, 1.6 Hz, 6H), Figure S2: ¹³C NMR spectrum of 4-(1,2,2-triphenylvinyl) benzaldehyde (75 MHz, CDCl₃): δ 191.86, 150.57, 143.07, 143.03, 142.92, 139.80, 134.33, 131.96, 131.30, 131.26, 130.90, 129.17, 127.95, 127.77, 127.08, 126.90, Figure S3: ESI mass spectrum of 4-(1,2,2-triphenylvinyl) benzaldehyde: *m/z* calculated mass for C₂₇H₂₀O *m/z* = 360.1 and found *m/z* = 361 [M+H]⁺, Figure S4: ¹H NMR spectrum of DTITPE (400 MHz, CDCl₃) δ 9.30 (s, 1H), 7.61 – 7.59 (m, 2H), 7.38 (s, 1H), 7.10 (td, *J* = 6.1, 3.3 Hz, 15H), 7.06 – 7.02 (m, 7H), Figure S5: ¹³C NMR spectrum of DTITPE (75 MHz, CDCl₃) δ 146.01, 143.52, 143.34, 140.21, 132.00, 131.43, 131.38, 131.34, 127.89, 127.80, 127.72, 126.74, 126.68, 124.79, Figure S6: MALDI-TOF mass spectrum for DTITPE: *m/z* calculated for C₃₇N₂₇S₂: 563.2; found: 563.6 [M+H]⁺, Figure S7: ¹H NMR spectrum of DTITPE.F⁻ (400 MHz, CDCl₃): δ 8.03 (d, *J* = 8.4 Hz, 2H), 7.40 (d, *J* = 2.9 Hz, 2H), 7.15 (dd, *J* = 5.1, 0.9 Hz, 2H), 7.12 – 7.04 (m, 10H), 7.04 – 6.97 (m, 6H), 6.94 (dd, *J* = 5.0, 3.6 Hz, 2H), Figure S8: ¹³C NMR spectrum of DTITPE.F⁻ (101 MHz, CDCl₃): δ 143.86, 143.78, 142.89, 140.90, 131.40, 131.37, 129.87, 127.72, 127.59, 127.10, 126.43, 126.37, 125.28, 124.09, Figure S9: MALDI-TOF mass spectrum for DTITPE⁻, calculated mass *m/z* = 561.15 and found *m/z* = 562.5 [M+H]⁺, Figure S10: FT-IR spectra of TITPE and TITPE.F⁻, Figure S11: Benesi–Hildebrand plot for the determination of the binding constant of DTITPE in THF using fluorescence emission data, Figure S12: Determination of the detection limit of DTITPE in THF using fluorescence emission data, Figure S13: Benesi–Hildebrand plot for the determination of the binding constant of DTITPE in THF using UV-vis. absorption data, Figure S14: Determination of the detection limit of DTITPE in THF using UV-vis. absorption data in THF, Figure S15: Determination of

the stoichiometric ratio between DTITPE and F^- in THF by Job's plot, Figure S16: a 1H NMR Spectra of DTITPE and DTITPE. F^- , b, 1H NMR spectrum of the molecular sensor DTITPE with incremental addition of TBAF, in $CDCl_3$ at room temperature, Figure S17: Optimized geometry of DTITPE, (b) Electrostatic potential (ESP) (isovalue = 0.02) surfaces of DTITPE, (c) Top view of DTITPE, and d) Side view of DTITPE, Figure S18: DFT optimized electronic distributions of DTITPE for various HOMO and LUMO energy levels, Figure S19: (a) Optimized geometry of DTITPE. F^- (b) Electrostatic potential (ESP) (isovalue = 0.02) surface of DTITPE. F^- (c) Top view of DTITPE. F^- , and (d) Side view of DTITPE. F^- , Figure S20: DFT optimized electronic distributions of DTITPE. F^- at various HOMO and LUMO energy levels, Figure S21: (a) Optimized geometry of deprotonated DTITPE $^-$, (b) The electrostatic potential (ESP) (isovalue = 0.02) surface of DTITPE $^-$, (c) Top view of DTITPE $^-$, and (d) Side view of DTITPE $^-$, Figure S22: DFT optimized electronic distributions of DTITPE $^-$ at various HOMO and LUMO energy levels, Figure S23: Theoretical UV-vis. spectra for DTITPE and DTITPE. F^- calculated using TD-DFT/B3LYP/6-31+G(d,p) with the CPCM method using THF as solvent, Table S1: Calculated bond lengths and dihedral angles of DTITPE, DTITPE. F^- and DTITPE $^-$ using B3LYP/6-31+G(d,p) method, Table S2: Calculated HOMO and LUMO energies and band gaps for DTITPE, DTITPE. F^- and DTITPE $^-$ calculated using B3LYP/6-31+G(d,p) method, Table S3: Theoretical energy levels and MO character for DTITPE, DTITPE. F^- and DTITPE $^-$ calculated using TD-DFT/B3LYP/6-31+G(d,p) with CPCM method using THF as solvent, Table S4: Comparison of the imidazole derived molecular sensors and their sensing properties, Table S5: Crystal data and structure refinement for DTITPE.

Author Contributions: Conceptualization, R.K.J.; Funding Acquisition, S.K.B.; Investigation, N.M., S.H.P., R.T.; Methodology, R.K.J.; Project Administration, N.M.; Supervision, S.K.B.; Visualization, G.R., A.K.V.; formal analysis, G.L.; Writing—original draft, R.K.J.; Writing—review & editing, S.H.P. All authors have read and agreed to the published version of the manuscript.

Funding: This work was financially supported by the CSIR-IICT (in-house project MLP-0007) and DST-(EMR/2016/006410).

Institutional Review Board Statement: Not applicable.

Informed Consent Statement: Not applicable.

Data Availability Statement: Data are contained within the article or supplementary material.

Acknowledgments: JRK is grateful to the IICT-RMIT Centre for the award of a Research Fellowship. The authors would like to thank J. Lakshmikanth Rao, C and FC Department, CSIR-IICT for conducting the DFT calculations. AKV acknowledges SERB-NPDF (PDF/2016/001158). We thank the Director, CSIR-IICT (No. IICT/Pubs./2020/183) for providing all the required facilities to carry out the work.

Conflicts of Interest: The authors declare that they have no known competing financial interests or personal relationships that could have appeared to influence the work reported in this paper.

References

1. Wu, N.; Zhao, L.-X.; Jiang, C.-Y.; Li, P.; Liu, Y.; Fu, Y.; Ye, F. A naked-eye visible colorimetric and fluorescent chemosensor for rapid detection of fluoride anions: Implication for toxic fluorine-containing pesticides detection. *J. Mol. Liq.* **2020**, *302*, 112549. [[CrossRef](#)]
2. Mukherjee, S.; Betal, S.; Chattopadhyay, A.P. A novel turn-on red light emitting chromofluorogenic hydrazone based fluoride sensor: Spectroscopy and DFT studies. *J. Photochem. Photobiol. A Chem.* **2020**, *389*, 112219. [[CrossRef](#)]
3. Xiao, L.; Ren, L.; Jing, X.; Li, Z.; Wu, S.; Guo, D. A selective naphthalimide-based colorimetric and fluorescent chemosensor for "naked-eye" detection of fluoride ion. *Inorg. Chim. Acta* **2020**, *500*, 119207. [[CrossRef](#)]
4. Yadav, P.; Kumari, M.; Jain, Y.; Agarwal, M.; Gupta, R. Antipyrine based Schiff's base as a reversible fluorescence turn "off-on-off" chemosensor for sequential recognition of Al^{3+} and F^- ions: A theoretical and experimental perspective. *Spectrochim. Acta Part A Mol. Biomol. Spectrosc.* **2020**, *227*, 117596. [[CrossRef](#)] [[PubMed](#)]
5. Bhat, M.P.; Kigga, M.; Govindappa, H.; Patil, P.; Jung, H.-Y.; Yu, J.; Kurkuri, M. A reversible fluoride chemosensor for the development of multi-input molecular logic gates. *New J. Chem.* **2019**, *43*, 12734–12743. [[CrossRef](#)]
6. Kumar, J.R.; Reddy, E.R.; Trivedi, R.; Vardhaman, A.K.; Giribabu, L.; Mirzadeh, N.; Bhargava, S.K. Isophorone-boronate ester: A simple chemosensor for optical detection of fluoride anion. *Appl. Organomet. Chem.* **2019**, *33*, e4688. [[CrossRef](#)]
7. Yalçın, E.; Alkış, M.; Seferoğlu, N.; Seferoğlu, Z. A novel coumarin-pyrazole-triazine based fluorescence chemosensor for fluoride detection via deprotonation process: Experimental and theoretical studies. *J. Mol. Struct.* **2018**, *1155*, 573–581. [[CrossRef](#)]

8. Sun, X.; Reuther, J.F.; Phillips, S.T.; Anslyn, E.V. Coupling activity-based detection, target amplification, colorimetric and fluorometric signal amplification, for quantitative chemosensing of fluoride generated from nerve agents. *Chem. A Eur. J.* **2017**, *23*, 3903–3909. [[CrossRef](#)]
9. Lohar, S.; Dhara, K.; Roy, P.; Babu, S.P.S.; Chattopadhyay, P. Highly sensitive ratiometric chemosensor and biomarker for cyanide ions in the aqueous medium. *ACS Omega* **2018**, *3*, 10145–10153. [[CrossRef](#)]
10. Kaushik, R.; Ghosh, A.; Singh, A.; Gupta, P.; Mittal, A.; Jose, D.A. Selective detection of cyanide in water and biological samples by an off-the-shelf compound. *ACS Sens.* **2016**, *1*, 1265–1271. [[CrossRef](#)]
11. Gale, P.A.; Busschaert, N.; Haynes, C.; Karagiannidis, L.E.; Kirby, I.L. Anion receptor chemistry: Highlights from 2011 and 2012. *Chem. Soc. Rev.* **2014**, *43*, 205–241. [[CrossRef](#)]
12. Wenzel, M.; Hiscock, J.R.; Gale, P.A. Anion receptor chemistry: Highlights from 2010. *Chem. Soc. Rev.* **2012**, *41*, 480–520. [[CrossRef](#)] [[PubMed](#)]
13. Na Kim, H.; Guo, Z.; Zhu, W.; Yoon, J.; Tian, H. Recent progress on polymer-based fluorescent and colorimetric chemosensors. *Chem. Soc. Rev.* **2011**, *40*, 79–93. [[CrossRef](#)]
14. Duke, R.; Veale, E.; Pfeffer, F.; Kruger, P.E.; Gunnlaugsson, T. Colorimetric and fluorescent anion sensors: An overview of recent developments in the use of 1, 8-naphthalimide-based chemosensors. *Chem. Soc. Rev.* **2010**, *10*, 3936–3953. [[CrossRef](#)]
15. Cho, D.-G.; Sessler, J.L. Modern reaction-based indicator systems. *Chem. Soc. Rev.* **2009**, *38*, 1647–1662. [[CrossRef](#)]
16. Moragues, M.E.; Martínez-Mañez, R.; Sancenón, F. Chromogenic and fluorogenic chemosensors and reagents for anions. A comprehensive review of the year 2009. *Chem. Soc. Rev.* **2011**, *40*, 2593–2643. [[CrossRef](#)]
17. Whitford, G.M. Acute Toxicity of Ingested Fluoride. *Monogr. Oral Sci.* **2011**, *22*, 66–80. [[CrossRef](#)] [[PubMed](#)]
18. Kirk, K.L. Biochemistry of Inorganic Fluoride. In *Biochemistry of the Elemental Halogens and Inorganic Halides*; Springer Science and Business Media LLC: Boston, MA, USA, 1991; pp. 19–68.
19. Kleerekoper, M. The role of fluoride in the prevention of osteoporosis. *Endocrinol. Metab. Clin. N. Am.* **1998**, *27*, 441–452. [[CrossRef](#)]
20. Briançon, D. Fluoride and osteoporosis: An overview. *Rev. Rhum.* **1997**, *64*, 78–81.
21. Pitt, P.; Berry, H. Fluoride treatment in osteoporosis. *Postgrad. Med. J.* **1991**, *67*, 323–326. [[CrossRef](#)]
22. Xu, S.; Chen, K.; Tian, H. A colorimetric and fluorescent chemodosimeter: Fluoride ion sensing by an axial-substituted subphthalocyanine. *J. Mater. Chem.* **2005**, *15*, 2676–2680. [[CrossRef](#)]
23. Konieczka, P.; Zygumt, B.; Namiesnik, J. Comparison of fluoride ion-selective electrode based potentiometric methods of fluoride determination in human urine. *Bull. Environ. Contam. Toxicol.* **2000**, *64*, 794–803. [[CrossRef](#)] [[PubMed](#)]
24. Christison, T.T.; Rohrer, J.S. Direct determination of free cyanide in drinking water by ion chromatography with pulsed amperometric detection. *J. Chromatogr. A* **2007**, *1155*, 31–39. [[CrossRef](#)]
25. Xu, Z.; Chen, X.; Na Kim, H.; Yoon, J. ChemInform Abstract: Sensors for the Optical Detection of Cyanide Ion. *ChemInform* **2010**, *41*, 127–137. [[CrossRef](#)]
26. Chung, Y.M.; Raman, B.; Kim, D.-S.; Ahn, K.H. Fluorescence modulation in anion sensing by introducing intramolecular H-bonding interactions in host–guest adducts. *Chem. Commun.* **2006**, *2*, 186–188. [[CrossRef](#)] [[PubMed](#)]
27. Safavi, A.; Maleki, N.; Shahbaazi, H. Indirect determination of cyanide ion and hydrogen cyanide by adsorptive stripping voltammetry at a mercury electrode. *Anal. Chim. Acta* **2004**, *503*, 213–221. [[CrossRef](#)]
28. Shan, D.; Mousty, C.; Cosnier, S. Subnanomolar cyanide detection at polyphenol oxidase/clay biosensors. *Anal. Chem.* **2004**, *76*, 178–183. [[CrossRef](#)]
29. Suzuki, T.; Hioki, A.; Kurahashi, M. Development of a method for estimating an accurate equivalence point in nickel titration of cyanide ions. *Anal. Chim. Acta* **2003**, *476*, 159–165. [[CrossRef](#)]
30. Rao, V.K.; Suresh, S.; Rao, N.; Rajaram, P. An electrochemical sensor for detection of hydrogen cyanide gas. *Bull. Electrochem.* **1997**, *13*, 327–329.
31. Itai, K.; Tsunoda, H. Highly sensitive and rapid method for determination of fluoride ion concentrations in serum and urine using flow injection analysis with a fluoride ion-selective electrode. *Clin. Chim. Acta* **2001**, *308*, 163–171. [[CrossRef](#)]
32. Luo, J.; Xie, Z.; Lam, J.W.Y.; Cheng, L.; Chen, H.; Qiu, C.; Kwok, H.S.; Zhan, X.; Liu, Y.; Zhu, D. Aggregation-induced emission of 1-methyl-1, 2, 3, 4, 5-pentaphenylsilole. *Chem. Commun.* **2001**, *18*, 1741.
33. Feng, G.; Yuan, Y.; Fang, H.; Zhang, R.; Xing, B.; Zhang, G.; Zhang, D.; Liu, B. A light-up probe with aggregation-induced emission characteristics (AIE) for selective imaging, naked-eye detection and photodynamic killing of Gram-positive bacteria. *Chem. Commun.* **2015**, *51*, 12490–12493. [[CrossRef](#)]
34. Zhang, L.; Hu, W.; Yu, L.; Wang, Y. Click synthesis of a novel triazole bridged AIE active cyclodextrin probe for specific detection of Cd²⁺. *Chem. Commun.* **2015**, *51*, 4298–4301. [[CrossRef](#)] [[PubMed](#)]
35. Zhao, Z.; He, B.; Tang, B.Z. Aggregation-induced emission of siloles. *Chem. Sci.* **2015**, *6*, 5347–5365. [[CrossRef](#)] [[PubMed](#)]
36. Mei, J.; Leung, N.L.C.; Kwok, R.T.K.; Lam, J.W.Y.; Tang, B.Z. Aggregation-induced emission: Together we shine, united we soar! *Chem. Rev.* **2015**, *115*, 11718–11940. [[CrossRef](#)] [[PubMed](#)]
37. Li, X.; Xu, B.; Lu, H.; Wang, Z.; Zhang, J.; Zhang, Y.; Dong, Y.; Ma, K.; Wen, S.; Tian, W. Label-free fluorescence turn-on detection of Pb²⁺ based on AIE-active quaternary ammonium salt of 9,10-distyrylanthracene. *Anal. Methods* **2013**, *5*, 438–441. [[CrossRef](#)]
38. Li, H.; Zhang, X.; Zhang, X.; Yang, B.; Wei, Y. Stable biocompatible cross-linked fluorescent polymeric nanoparticles based on AIE dye and itaconic anhydride. *Colloids Surf. B* **2014**, *121*, 347–353. [[CrossRef](#)]

39. Liu, X.; Zeng, Y.; Liu, J.; Li, P.; Zhang, D.; Zhang, X.; Yu, T.; Chen, J.; Yang, G.; Li, Y. Highly emissive nanoparticles based on aie-active molecule and pamam dendritic “molecular glue”. *Langmuir* **2015**, *31*, 4386–4393. [[CrossRef](#)] [[PubMed](#)]
40. Chen, M.; Nie, H.; Song, B.; Li, L.; Sun, J.Z.; Qin, A.; Tang, B.Z. Triphenylamine-functionalized tetraphenylpyrazine: Facile preparation and multifaceted functionalities. *J. Mater. Chem. C* **2015**, *4*, 2901–2908. [[CrossRef](#)]
41. Guo, Z.; Shao, A.; Zhu, W.-H. Long wavelength AIEgen of quinoline-malononitrile. *J. Mater. Chem. C* **2015**, *4*, 2640–2646. [[CrossRef](#)]
42. Li, N.; Feng, H.; Gong, Q.; Wu, C.; Zhou, H.; Huang, Z.; Yang, J.; Chen, X.; Zhao, N. BINOL-based chiral aggregation-induced emission luminogens and their application in detecting copper(II) ions in aqueous media. *J. Mater. Chem. C* **2015**, *3*, 11458–11463. [[CrossRef](#)]
43. Shan, G.-G.; Li, H.-B.; Sun, H.-Z.; Zhu, D.-X.; Cao, H.-T.; Su, Z.-M. Controllable synthesis of iridium(III)-based aggregation-induced emission and/or piezochromic luminescence phosphors by simply adjusting the substitution on ancillary ligands. *J. Mater. Chem. C* **2013**, *1*, 1440–1449. [[CrossRef](#)]
44. Ding, D.; Li, K.; Liu, B.; Tang, B.Z. Bioprobes based on AIE fluorogens. *Acc. Chem. Res.* **2013**, *46*, 2441–2453. [[CrossRef](#)] [[PubMed](#)]
45. Molina, P.; Tárraga, A.; Otón, F. Imidazole derivatives: A comprehensive survey of their recognition properties. *Org. Biomol. Chem.* **2012**, *10*, 1711–1724. [[CrossRef](#)]
46. Cheng, D.; Liu, X.; Yang, H.; Zhang, T.; Han, A.; Zang, L. A Cu²⁺-selective probe based on phenanthro-imidazole derivative. *Sensors* **2016**, *17*, 35. [[CrossRef](#)] [[PubMed](#)]
47. Wang, B.; Lv, X.; Pan, B.; Tan, J.; Jin, J.; Wang, L. Benzimidazole–phosphine oxide hybrid electron transporters for unilateral homogeneous phosphorescent organic light-emitting diodes with enhanced power efficiency. *J. Mater. Chem. C* **2015**, *3*, 11192–11201. [[CrossRef](#)]
48. Guo, Z.; Song, N.R.; Moon, J.H.; Kim, M.; Jun, E.J.; Choi, J.; Lee, J.Y.; Bielawski, C.W.; Sessler, J.L.; Yoon, J. A benzobisimidazolium-based fluorescent and colorimetric chemosensor for CO₂. *J. Am. Chem. Soc.* **2012**, *134*, 17846–17849. [[CrossRef](#)]
49. Wu, Y.; Huo, J.-P.; Cao, L.; Ding, S.; Wang, L.-Y.; Cao, D.; Wang, Z.-Y. Design and application of tri-benzimidazolyl star-shape molecules as fluorescent chemosensors for the fast-response detection of fluoride ion. *Sens. Actuators B Chem.* **2016**, *237*, 865–875. [[CrossRef](#)]
50. Swami, S.; Behera, D.; Agarwala, A.; Verma, V.P.; Shrivastava, R. β -Carboline–imidazopyridine hybrids: Selective and sensitive optical sensors for copper and fluoride ions. *New J. Chem.* **2018**, *42*, 10317–10326. [[CrossRef](#)]
51. Tabasi, Z.A.; Younes, E.; Walsh, J.C.; Thompson, D.W.; Bodwell, G.J.; Zhao, Y. Pyrenoidimidazolyl-benzaldehyde fluorophores: Synthesis, properties, and sensing function for fluoride anions. *ACS Omega* **2018**, *3*, 16387–16397. [[CrossRef](#)]
52. Manivannan, R.; Satheskumar, A.; Elango, K.P. Tuning of the H-bonding ability of imidazole N–H towards the colorimetric sensing of fluoride and cyanide ions as their sodium salts in water. *New J. Chem.* **2013**, *37*, 3152–3160. [[CrossRef](#)]
53. Causey, C.P.; Allen, W.E. Anion binding by fluorescent biimidazole diamides. *J. Org. Chem.* **2002**, *67*, 5963–5968. [[CrossRef](#)]
54. Cui, Y.; Mo, H.-J.; Chen, J.-C.; Niu, Y.-L.; Zhong, Y.-R.; Zheng, K.-C.; Ye, B.-H. Anion-selective interaction and colorimeter by an optical metalloreceptor based on ruthenium(II) 2,2'-biimidazole: Hydrogen bonding and proton transfer. *Inorg. Chem.* **2007**, *46*, 6427–6436. [[CrossRef](#)] [[PubMed](#)]
55. Zhan, C.-G.; Nichols, J.; Dixon, D.A. Ionization potential, electron affinity, electronegativity, hardness, and electron excitation energy: Molecular properties from density functional theory orbital energies. *J. Phys. Chem. A* **2003**, *107*, 4184–4195. [[CrossRef](#)]
56. Naha, S.; Velmathi, S.J.C. Phenazine-based fluorescence “turn-off” sensor for fluoride: Application on real samples and to cell and zebrafish imaging. *ChemistrySelect* **2019**, *4*, 2912–2917. [[CrossRef](#)]
57. Bhattacharyya, B.; Kundu, A.; Guchhait, N.; Dhara, K. Anthraimidazole based reversible and reusable selective chemosensors for fluoride ion: Naked-eye, colorimetric and fluorescence “ON-OFF”. *J. Fluoresc.* **2017**, *27*, 1041–1049. [[CrossRef](#)]
58. Yang, Z.; Chi, Z.; Mao, Z.; Zhang, Y.; Liu, S.; Zhao, J.; Aldred, M.P.; Chi, Z. Recent advances in mechano-responsive luminescence of tetraphenylethylene derivatives with aggregation-induced emission properties. *Mater. Chem. Front.* **2018**, *2*, 861–890. [[CrossRef](#)]
59. Sagara, Y.; Kato, T. Mechanically induced luminescence changes in molecular assemblies. *Nat. Chem.* **2009**, *1*, 605–610. [[CrossRef](#)]
60. Sagara, Y.; Kubo, K.; Nakamura, T.; Tamaoki, N.; Weder, C. Temperature-dependent mechanochromic behavior of mechanoreponsive luminescent compounds. *Chem. Mater.* **2017**, *29*, 1273–1278. [[CrossRef](#)]
61. Chi, Z.G.; Zhang, X.Q.; Xu, B.J.; Zhou, X.; Ma, C.P.; Zhang, Y.; Liu, S.W.; Xu, J.R. Recent advances in organic mechanofluorochromic materials. *Chem. Soc. Rev.* **2012**, *41*, 3878–3896. [[CrossRef](#)]
62. Liang, J.; Chen, Z.; Xu, L.; Wang, J.; Yin, J.; Yu, G.-A.; Chen, Z.-N.; Liu, S.H. Aggregation-induced emission-active gold(I) complexes with multi-stimuli luminescence switching. *J. Mater. Chem. C* **2014**, *2*, 2243–2250. [[CrossRef](#)]
63. Yang, X.; Zheng, L.; Xie, L.; Liu, Z.; Li, Y.; Ning, R.; Zhang, G.; Gong, X.; Gao, B.; Liu, C.; et al. Colorimetric and On–Off fluorescent chemosensor for fluoride ion based on diketopyrrolopyrrole. *Sens. Actuators B Chem.* **2015**, *207*, 9–24. [[CrossRef](#)]
64. Yang, X.; Xie, L.; Ning, R.; Gong, X.; Liu, Z.; Li, Y.; Zheng, L.; Zhang, G.; Gao, B.; Cui, Y.; et al. A diketopyrrolopyrrole-based near-infrared sensor for selective recognition of fluoride ions. *Sens. Actuators B Chem.* **2015**, *210*, 784–794. [[CrossRef](#)]
65. Reddy, T.S.; Maragani, R.; Misra, R. Triarylborane substituted naphthalimide as a fluoride and cyanide ion sensor. *Dalton Trans.* **2015**, *45*, 2549–2553. [[CrossRef](#)]
66. Hutchison, G.; Ratner, M.A.; Marks, T.J. Intermolecular charge transfer between heterocyclic oligomers. effects of heteroatom and molecular packing on hopping transport in organic semiconductors. *J. Am. Chem. Soc.* **2005**, *127*, 16866–16881. [[CrossRef](#)] [[PubMed](#)]